Available online at www.sciencedirect.com
SCIENCE DIRECT®
PERGAMON
International Journal of Rock Mechanics & Mining Sciences 40 (2003) 1225–1241
International Journal of Rock Mechanics and Mining Sciences
www.elsevier.com/locate/ijrmms

Electrical imaging and hydraulic testing for a complete stress determination

F.H. Cornet*, M.L. Doan, F. Fontbonne

Département de Sismologie, Institut de Physique du Globe de Paris, Universite Pierre et Marie Curie, 4 Place Jussieu, Paris, Cedex 05 75230, France

Accepted 30 June 2003

Abstract

A complete stress determination has been performed in Lodève (southern France) by conducting hydraulic tests in a 200 m deep borehole, with a probe combining electrical imaging with an inflatable straddle packer. Both classical hydraulic fracturing and hydraulic tests on pre-existing fractures have been conducted. The normal stress acting on the tested fracture planes was determined from the simultaneous analysis of both hydraulic and electrical signals observed during shut-in phases. Values derived from quasi-static reopening pressure tests are systematically larger than those derived from shut-in and have been discarded. Hydraulic fractures provide information on the principal stress directions orientation as well as on the minimum principal stress magnitude. HTPF tests provide information on the vertical and the maximum horizontal principal stress components magnitude and are unaffected by any pore pressure effect. At a depth of $z = 165$ m, the vertical stress component is principal and is given by $S_v = 4.0 \pm 0.5$ MPa. The maximum horizontal principal component is oriented N155° $\pm$ 10° and is given by $S_H = 10.0 \pm 0.2$ MPa. It is almost twice the value found for S_h, $S_h = 5.8 \pm 0.1$ MPa. These results are consistent with the results obtained nearby. They show that hydraulic properties of faults (discontinuities with length larger than 1 km and offsets larger than 100 m) do not depend simply on the relative orientation of the fault with respect to the principal stress directions.

Keywords: Stress determination; Hydraulic methods; Inverse problem; Probability density function; Electrical monitoring

1. Introduction

The determination of stresses at distances greater than 100 m from a free surface, whether it is the ground surface or that of an underground cavity, is often conducted by hydraulic tests in boreholes. Two techniques are commonly used for such stress determinations, the hydraulic fracturing (HF) technique and the hydraulic tests on pre-existing fractures (HTPF) or hydraulic jacking technique.

With the classical HF stress determination technique [1,2], the borehole used for the stress determination is assumed to be parallel to one of the principal stress directions. Validity of this assumption is ascertained by the fracture traces observed after testing, at the borehole wall. Indeed, when the borehole axis is inclined by more than 15° with respect to a principal stress direction, en echelon fractures are observed [3,4]. In the best cases (when induced fractures are parallel to the borehole axis, thus demonstrating parallelism between the borehole axis and a principal stress direction), a hydraulic fracturing yields five out of the six stress tensor components, namely the three Euler angles and the magnitude of the principal stress components in directions perpendicular to the borehole axis. Yet, even in these ideal conditions, some large uncertainty affects the determination of the magnitude of the maximum stress component perpendicular to the borehole axis because of difficulties with characterizing both the tensile strength of the material and the effect of interstitial pressure [5–7]. So, with the HF technique, only four components are determined with certainty, the three Euler angles and the minimum principal stress magnitude.

The HTPF technique [9,10], sometimes called hydraulic jacking technique [11] or the fracture pressurization technique [12,13] aims at measuring the normal stress component supported by pre-existing fractures. It does not require any a priori hypothesis on the relative orientation of the borehole axis. But it requires testing at least eight or nine fractures with six different

*Corresponding author.
E-mail address: cornet@ipgp.jussieu.fr (F.H. Cornet).

1365-1609/$ - see front matter © 2003 Elsevier Ltd. All rights reserved.
doi:10.1016/S1365-1609(03)00109-6

orientations for a complete stress tensor determination, because of the need of redundancy to compensate for uncertainties. Furthermore, when the distance between the fractures is large as compared to the stress gradient in the formation, some additional hypothesis is formulated for the stress variation within the volume under investigation. Then, because more parameters are required for describing the stress field, a larger number of fractures must be tested. Typically, in a mountainous environment where only one borehole is available and no a priori guess can be formulated for the principal stress directions, between 15 and 20 successful hydraulic tests are required for obtaining a fair appraisal of the local stress tensor and its local variation along the borehole axis [14].

Combining both HF and HTPF keeps the amount of tests at a minimum and yet provides a complete determination of the stress tensor. We report in this paper a case example where it has been possible to associate both HF and HTPF tests for such a complete stress determination. The motivation for this stress determination was to investigate the specific orientation of the most water-producing fractures with respect to the regional stress field in an underground mine. The site of the stress measurements (COGEMA borehole nb 121) is located in St Jean de la Blaquière (N43° 42′42″, E3° 26′22″ in WGS84 datum), near Lodève, in Southern France (see Fig. 1). The geological formation is a series of decimetric to centimetric beds of sandstone and pellites. A total of seven, 2.5 m long, borehole intervals have been hydraulically tested. Three tests have yielded true hydraulic fractures while four tests have led to the reopening of pre-existing fractures.

We describe first the method used for identifying the test intervals and the fracture orientation. Then the hydraulic tests results are presented and discussed together with a novel electrical method used for refining the normal stress determination. Finally, HF and HTPF results are integrated in a single best fitting solution.

2. Selection of test intervals and fracture orientation determination

Tests were run with the HTPF tool, which associates electrical borehole imaging for fracture reconnaissance with straddled inflatable packers for hydraulic testing [15–17]. Electrical imaging is used first for logging the

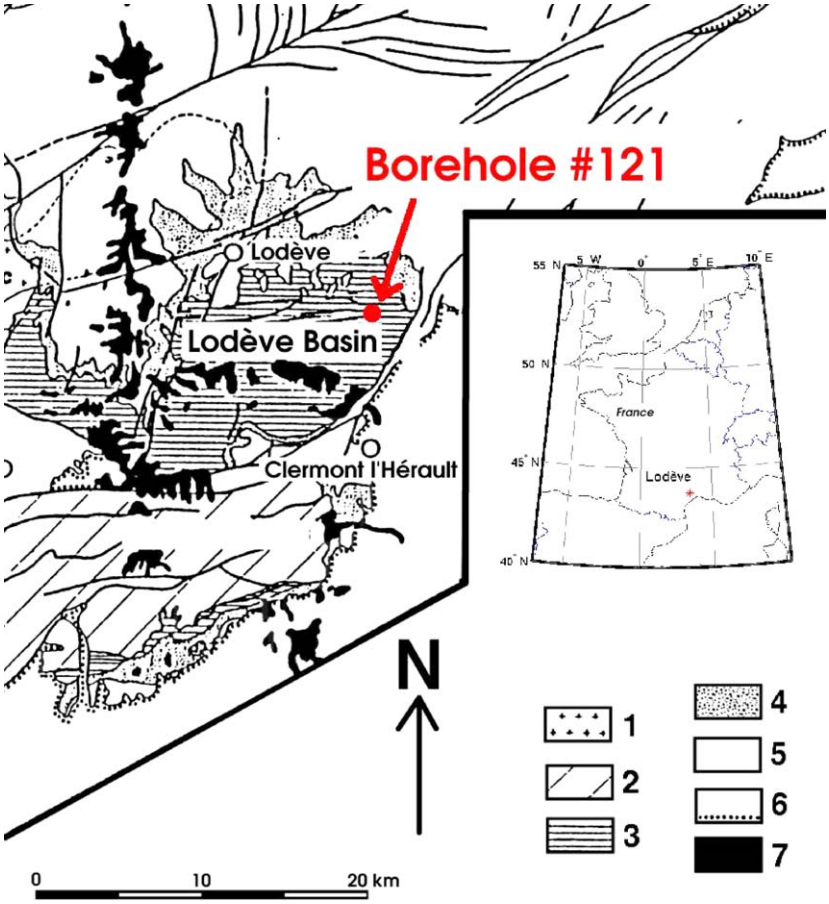

Fig. 1. Geological map of the Permian Lodève basin, southern France. 1—Mendic Granite, 2—Pre-Stephanian sedimentary sequence, involved in Hercynian tectonic. 3—Permian, 4—Trias, 5—Jurassic, 6—Tertiary and Quaternary sequences, 7—Plio-quaternary alcaline basalts of the Escandorgue. After [8].

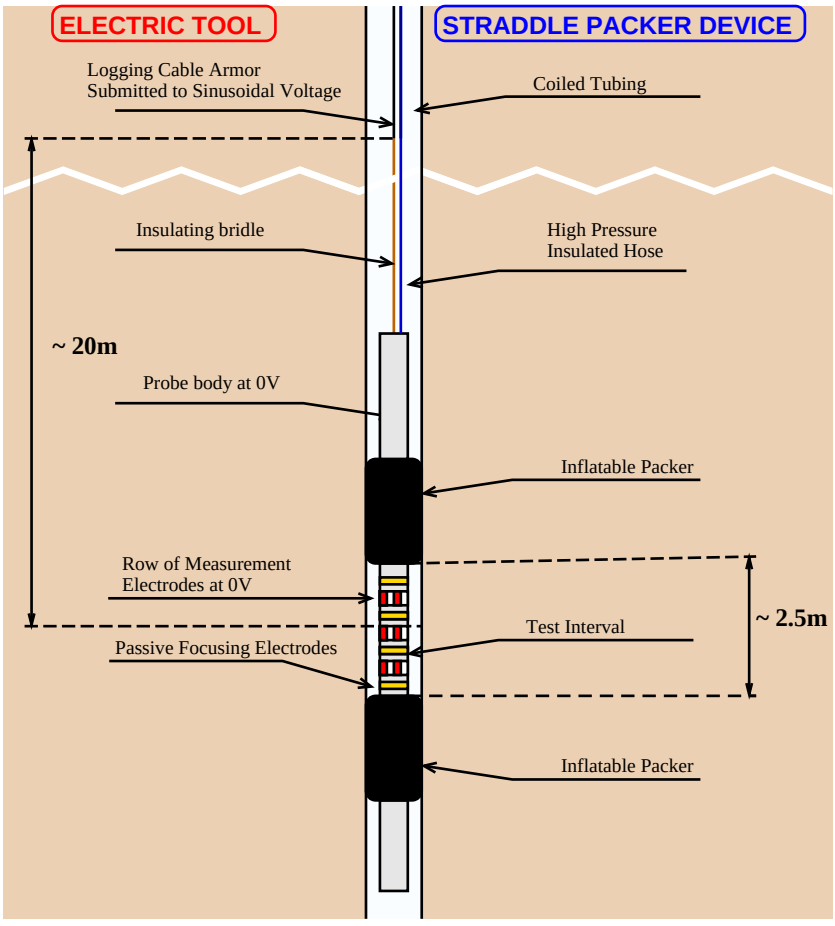

Fig. 2. Schematic diagram of the large diameter HTPF tool.

borehole and identifying the optimum location of test intervals (homogeneous rock formation for HF tests, single isolated fractures for HTPF tests). Then it provides means to identify the geometry of hydraulically tested fractures.

Fig. 2 shows a schematic sketch of this probe. It is operated with a 7-conductor logging cable separated from the tool itself by a 20-m long electrical insulating bridle. An alternating electrical current is applied between the metallic armor of the logging cable and the body of the tool. Focusing electrodes ensure that electrical current lines converge normally to the tool at measuring electrodes. These are distributed along 10 rows, which contain each a set of 16 evenly distributed electrodes. They are dispatched within the interval straddled by the two inflatable packers. Hence, each row of electrodes provides a measurement of azimuthal variations in electrical resistivity. When the tool is moved along the borehole, it provides a complete log of electrical resistivity variations at the borehole wall. It is also called an azimuthal laterolog. Such a log outlines, in particular, pre-existing fractures (Fig. 3). When the tool is fixed by the inflated packers, it provides means to map changes in electrical resistivity within the straddled interval.

Presently, two types of HTPF tools are available: one for slim boreholes (open-hole diameter ranging from 76 to 150 mm) and one for larger diameter boreholes (between 150 and 200 mm). The large diameter tool has been used for the present study. With the slim diameter tool, only one row of 24 electrodes is available and electrodes are dispatched below the straddled interval. Hence, the slim tool does not provide a real-time image of the straddled interval but only images before and after hydraulic testing [18].

2.1. Selection of test intervals

Fractures are easily recognized as sinusoids on electrical imaging logs. Their electrical resistivity is affected by both their filling composition and their hydraulic properties, so that some a priori geological information is necessary for interpreting correctly their electrical signature. For instance, clay seals hermetically a fracture but it is a very good electrical conductor. However, in many instances, electrically conductive fractures are also hydraulically permeable. When they are identified in otherwise homogeneous zones, they are the most amenable to hydraulic testing for normal stress measurements. Hence, electrical imaging provides the

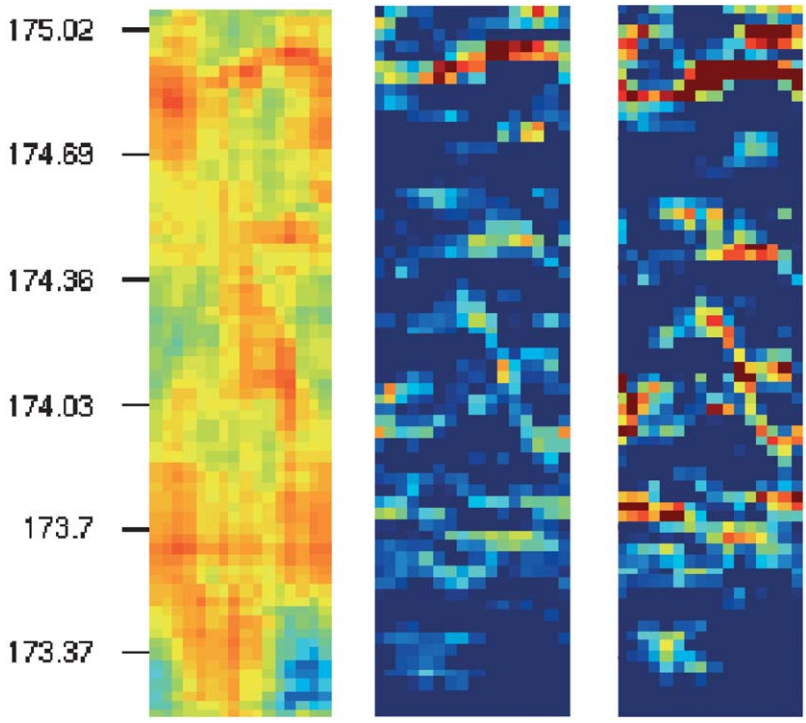

Fig. 3. Borehole imaging provided by the electrical device of the HTPF tool. For imaging logs, the quality of the raw image (left) is improved by plotting pixel vertical gradients (middle) and by stacking the data (right).

relevant data for the selection of zones to be hydraulically tested.

In Fig. 3 the image to the left shows the raw image as displayed on site, in real time. Its quality is sufficient to distinguish the main features of the borehole section. This 'fingerprint' is extremely valuable for positioning rapidly the tool exactly on the well interval to be tested, with a relative accuracy of a few centimeters. As depth errors with wireline logs can reach several meters at depths larger than 1000 m, this feature is extremely useful for positioning the tool precisely on selected intervals and also for comparisons between pre-test and post-test images. However, eccentering effects, low resistivity contrast and electronic noise alter the resolution of the image and signal processing is needed to exploit this log further.

HF interpretation supposes indeed that fracture propagates in a homogeneous zone, whereas HTPF results are disturbed by the presence of secondary fractures. These considerations require refined analyses, which rest on a greater resolution than that provided by the raw image. For instance, in Fig. 3, whereas the raw image displays a single fracture within the mapped section, the improved image shown in the center indicates a secondary intersecting fracture, which disqualifies this zone for further hydraulic testing. This improved image is obtained by computing the axial gradient of the image, i.e. the differences in values recorded by the electrodes of a given row, at two successive sampling times. This crude processing can also be conducted in the field. It eliminates most of the tool eccentering effects seen on the raw image and provides very satisfactory results in low resistivity contrast environment. But it is sensitive to low signal-to-noise ratio.

Image can also be improved by stacking the electrical currents recorded by all electrodes passing in the same azimuth and depth, at different times, during the logging operation (image to the right, in Fig. 3). The contrast gets sharper so that the sinusoidal line delineating a fracture is much narrower. This yields a more accurate measure of fracture orientation. A resolution of about 5° is obtained.

2.2. Electrical monitoring of hydraulic tests

The electrical imaging device provides real-time information *during* a hydraulic test. A typical hydraulic test is sequenced as indicated in Figs. 4 and 7: After a first breakdown and shut-in sequence, the fracture is successively opened and closed twice. Opening is performed through incremental constant pressure steps, which last 5 min each, and is followed by the shut-in phase. Such a procedure yields, in addition to the initial breakdown pressure, three readings for the shut-in pressure and two readings for the quasi-static reopening. A complete hydraulic test lasts from 90 to 120 min, including inflation and deflation of the packers.

This hydraulic testing of the fracture has some effects on the mean intensity recorded by the 160 electrodes.

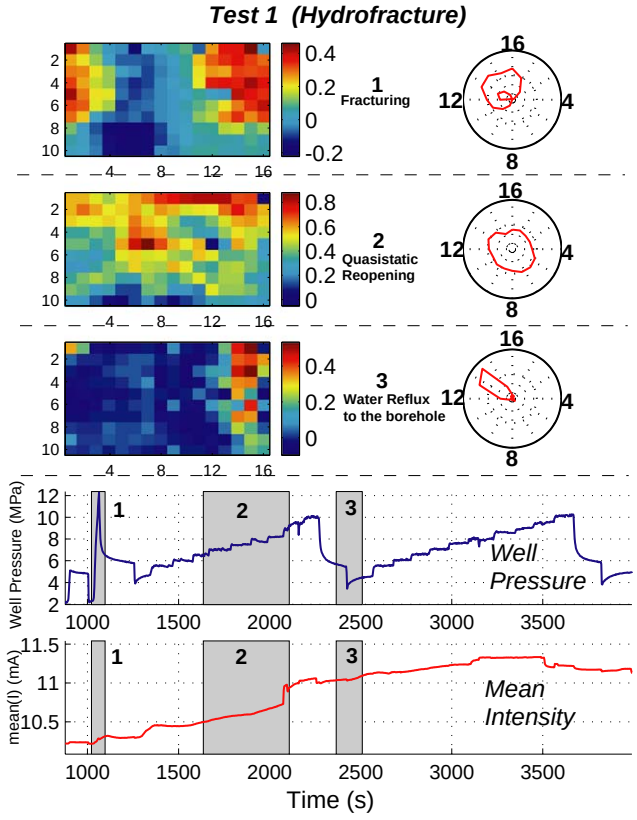

Fig. 4. Variations of electrical signal during three different steps of a hydraulic test. The change in electrical current distribution is displayed on the upper left corner. The intensity received by the 10 electrodes of a given column are summed. The 16 values so obtained are plotted on the polar diagram shown in the upper right corner. On the bottom graphs, variations of the mean electrical intensity are plotted versus time and can be compared to injection pressure variations.

A case example is exhibited at the bottom graph of Fig. 4, in which the time variations of the mean electrical intensity recorded by all electrodes during the hydraulic test are plotted. It highlights two phenomena: a continuous increase in electrical intensity and sharp surges correlated to key hydraulic stages.

Given the high permeability of the pelite, the first trend is interpreted as the effect of water percolation into the host rock as well as in the fracture. Indeed, such a continuous increase is not observed in impervious formation like granite [17]. It induces a progressive blur of images of the fracture, as shown in Fig. 4. Since, generally, the injected water has a lower salinity than the host formation, it outlines changes in pore volume associated with increase in pore pressure. Further analysis requires a sound measurement of the electrical conductivity of both the formation fluid and the injected water.

We will focus on the second trend which reveals itself very helpful for stress determination purposes. Electrical intensity soars during the breakdown ($t = 1000$ s) and the two quasi-static reopening stages ($t = 2000$ and 3100 s). In addition, when the system is drained at the end of a shut-in sequence ($t = 1250$ and 2500 s), water flow-back into the borehole is also associated with surges in electrical current. But the shut-in sequences are accompanied by a small drop of the electrical resistivity ($t = 1250$ and 2200 s).

This general trend is seen with more details with the real-time imaging provided by the electrical device. The three examples shown in Fig. 4 are computed from the differences between the final and the initial images for the corresponding time interval. Some regions appear to be more sensitive to pressure variations. They are consistent with the hydrofracture orientation given by the post-test imaging. Surprisingly enough, the best resolution for the fracture geometry is provided by imaging during the water flow-back period (step 3) rather than by the fracture opening phases. This may reflect the difference in salinity between the injected water and the formation fluid.

The first image of Fig. 4 corresponds to the breakdown phase. It shows an asymmetry in fracture opening. Only one branch of the fracture is opened, resulting in a large positive zone. The second branch of the fracture is visible only at the end of the second opening (step 2). Such asymmetric opening occurred for all hydrofracture operations performed during this campaign. In addition, electrical imaging also shows that pore pressure perturbation around the well is not axisymmetrical so that theoretical poroelastic models used for interpreting the breakdown pressure in terms of maximum horizontal principal stress may be strongly biased.

The relevance of electrical data for understanding the water percolation process is also well illustrated by the second test. The hydraulic graph of Fig. 6 indicates the existence of a highly hydraulically conductive zone within the straddled interval. Indeed, first the pressure does not hold during the initial permeability test. Second, the well pressure returns to the hydrostatic pressure during the shut-in period. Yet packer pressure remains always larger than the interval pressure, which prevents any leak through the packers.

Real-time electrical imaging helps identify the zone where flow occurs. It is indeed identified in the top left image of Fig. 6 as a local positive anomaly on rows 5 and 6. This positive anomaly (increase in conductivity) is just above the fracture trace. A better resolution for the fracture trace is provided by the pre- and post-frac imaging logs (see Fig. 5). The various increases and decreases in electrical resistivity eventually lead to the top right image of Fig. 6. In this figure, the anomaly seen during the first reopening is no more visible, while the fracture displays an heterogeneous resistivity variation: the lower section of the fracture exhibits a decrease in electrical conductivity while that of its upper section is sharply increased.

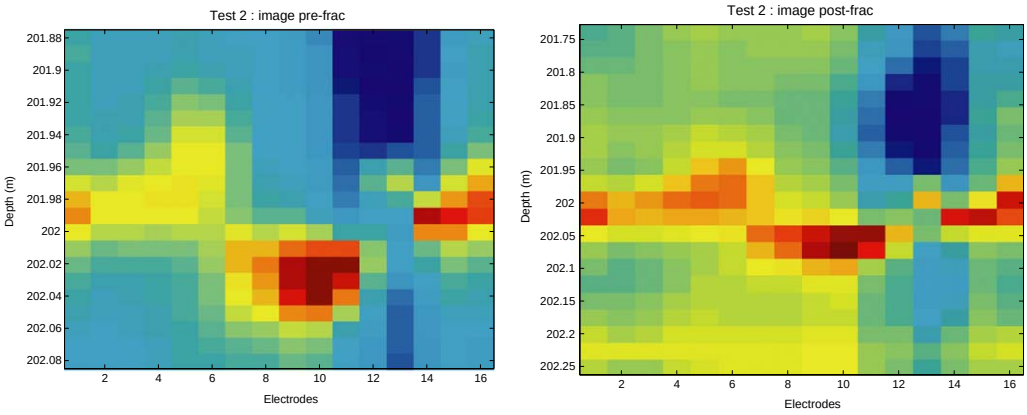

Fig. 5. Imaging of the second tested fracture before (left) and after (right) the hydraulic test.

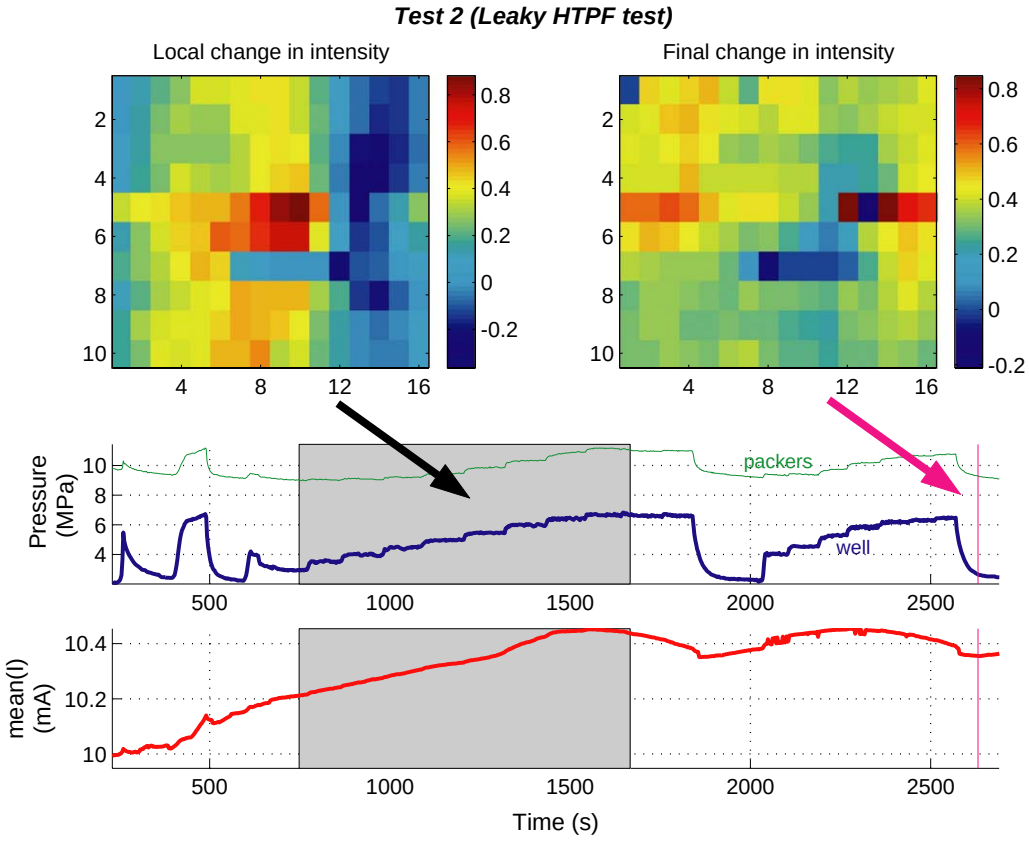

Fig. 6. Electrical variations observed during the second test. During the reopening test (left), a positive anomaly appears. At the end of the test, the image of the final changes exhibits the tested fracture.

This observation shows that the tested zone has effectively been affected by the pressure variation imposed during the hydraulic test. But the geometry of the flowing zone is that of channels with variable geometry and not that of an infinite planar fracture. Its hydraulic conductivity does depend on water pressure but its geometry is not compatible with the HTPF requirement of "infinite" planar fracture. It will be shown in the next section that the associated hydraulic curves do not provide relevant information on the regional stress field.

These two examples demonstrate that electrical signals provide an independent information on the percolation processes that occur during a hydraulic test. They help to ascertain the validity of hypothesis underlying the interpretation of hydraulic tests. They also produce complementary data for determining the normal stress applied to planar fractures, as described in the following section.

3. Normal stress determination

With the HTPF technique, the hydraulically tested fracture is used as a hydraulic flat-jack. The objective is to measure the pressure necessary to maintaining barely opened the fracture, i.e. the pressure which balances the normal stress acting onto the fracture. The strategy for getting this value is presented in Fig. 7 and has been described in the previous section. It is based on shut-in and quasi-static reopening phases. The testing procedure provides three, or more, shut-in and two quasi-static reopening phases, i.e. a minimum of five measurements of the normal stress supported by a given fracture, whether it was pre-existing to the testing or artificially developed by hydraulic fracturing.

3.1. Normal stress measurements during shut-in phases

Many methods have been proposed for retrieving the normal stress supported by a fracture from the pressure decay observed during the shut-in phase, at the end of a hydraulic injection test (see [19,20] for a review). To be meaningful, these tests must of course have been conducted at injection pressures larger than this far field normal stress. This will be discussed further when Lodève results are presented. Here, we have adopted two commonly used techniques, that proposed by Aamodt and Kuriyagawa [21], and that proposed by Hayashi and Haimson [19].

In addition, as discussed here above, the opening and closing of fractures have signatures in the intensity of the electrical current recorded with the HTPF tool. Doan and Cornet [22] have proposed a new method based on analysis of this electrical signal for pointing out the time when the fracture closes. Results are compared to those retrieved from the pressure decay analysis.

3.1.1. Determination from borehole pressure decay

Aamodt and Kuriyagawa's logarithmic fit

Aamodt and Kuriyagawa [21] studied large-scale hydraulic fractures. They noticed that the final part of the pressure decay fits well a negative exponential equation:

$$P = e^{-at+b} + P_a, \tag{1}$$

where a, b are empirical constants. P_a was designated as the pore fluid pressure near the borehole. They suggested that the departure of the exponential fit from the experimental curve yields the shut-in pressure.

Practically, $\ln(P - P_0) = f(t)$ is plotted for various values of P_0. A Taylor expansion of Eq. (1) demonstrates that, if $P_0 < P_a$, the curve is not monotonic, whereas choosing $P_0 > P_a$ yields a graph similar to Fig. 8. This serves as criterion for the determination of the reference pressure, P_a.

A linear regression is then computed from the final section of the hydraulic curve. Its departure from the

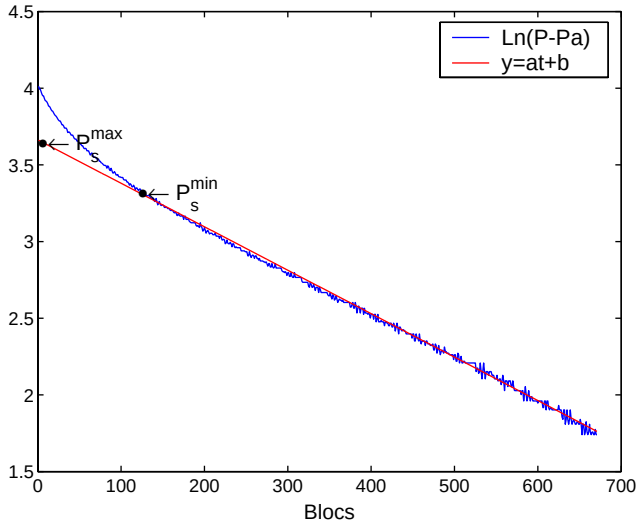

Fig. 8. Linear regression of the curve $\ln(P - P_a) = f(t)$ in the closed fracture regime.

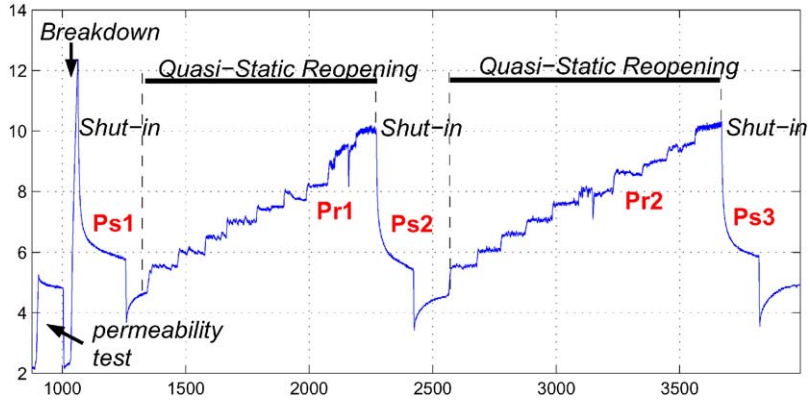

Fig. 7. Hydraulic sequences of the first hydraulic test of the Lodève campaign. After a preliminary permeability test, the fracture is fully opened. The fracture is then successively opened and closed. Note that the reopening is performed through quasi-static steps.

experimental curve provides the smallest acceptable value for the shut-in pressure P_s^{min}. The maximum estimate of shut-in pressure P_s^{max} is provided by extrapolation to the beginning of the shut-in process (see Fig. 8).

Table 1 reports the P_0 values observed for all the seven tests of the Lodève campaign. Values are fairly scattered and cannot be assimilated to the local far field pore pressure. This suggests that a permanent regime was not yet achieved at the end of the shut-in phase. Aamodt and Kuriyagawa [21] indeed applied their criterion to large-scale tests, with hours-long shut-in. The 5-min time-lapse adopted during the tests in Lodève is insufficient to attribute a simple physical meaning to the value of P_a.

Table 1
Values of the asymptotic pressure value, P_a, for all seven hydraulic tests of Lodève campaign

Test	1	2	3	4	5	6	7
P_0 (MPa)	5.5	2.2	4.8	5.0	4.0	4.7	2.2

Fortunately, the measured shut-in pressures are little sensitive to the choice of P_0.

Hayashi and Haimson's method

Hayashi and Haimson [19] consider also the shut-in of hydraulic fractures, i.e. symmetrical axial tensile fractures. They identify three phases during the shut-in process: (1) a phase during which fracture stops propagating, (2) a phase during which the fracture closes back progressively, and (3) a phase during which the fracture is closed and flow depends solely on the permeability of the formation. From the conservation of mass inside the fracture and the borehole, they obtain approximate equations describing the pressure decay and conclude that for the first and third phases, the inverse of the rate of pressure decay is approximately linear with respect to the test interval pressure. If P_1 is the borehole pressure at the end of crack growth (phase 1) and P_2 is the borehole pressure at the completion of

Table 2
Normal stress determination obtained by each stress determination method

Test depth (m)	Cycle number	Quasi-static reopening method		Aamodt and Kuriyagawa method		Hayashi and Haimson method		Electrical method		σ_n	$3\delta\sigma_n$
		P^R	$3\delta P^R$	P_m^A	P_M^A	P_m^H	P_M^H	P^E	$3\delta P^E$		
	1			6.2	6.6	6.9	7.1	6.4	0.2		
205	2	8.2	0.5	5.9	6.3	6.8	6.9	6.1	0.2	6.3	0.3
	3			6.3	6.9	7.0	7.3	NSV	x		
	1			2.6	3.3	3.3	3.6	3.4	0.6		
202	2	5.1	0.4	2.3	2.8	2.8	3.1	3.3	0.7	3.0	0.6
	3			2.5	3.2	3.3	3.6	3.2	0.9		
	1			6.4	7.6	6.9	7.1	7.4	0.2		
187	2	8.1	0.6	6.5	7.1	6.9	7.3	6.4	0.7	7.0	0.5
	3			6.5	6.9	7.1	7.3	6.6	0.3		
	1			7.0	8.1	7.5	7.7	NSV	x		
146	2	8.5	0.5	6.4	7.0	6.9	7.1	6.6	0.4	6.7	0.3
	3			7.0	7.2	7.0	7.2	6.6	0.4		
	4			6.18	6.9	6.9	7.0	NSV	x		
	1			4.7	5.2	5.2	5.6	4.8	0.6		
	2			4.6	5.0	5.2	5.6	4.8	0.6		
122	3	6.2	0.5	4.9	5.3	5.3	5.7	4.8	0.2	5.2	0.5
	4			5.4	5.7	5.5	5.8	4.8	0.2		
	5			5.4	5.7	5.6	5.8	5.2	0.5		
	1			5.1	5.5	5.1	5.2	5.5	0.3		
106	2	6.3	0.5	5.7	6.1	5.9	6.0	5.3	0.3	5.4	0.3
	3			5.5	5.8	5.7	5.8	5.2	0.1		
	4			5.7	5.9	5.8	5.9	5.4	0.2		
	1			2.8	3.02	2.9	3.1	2.7	0.2		
93	2	3.4	0.3	2.8	2.9	2.9	3.01	2.9	0.1	2.9	0.1
	3			2.9	3.0	2.9	3.0	2.9	0.1		

From left to right: quasi-static reopening (estimated from all the reopening sequences) [9], Aamodt and Kuriyagawa [21], Hayashi and Haimson [19], Doan and Cornet [22]. NSV means that no sharp variations were noticed in the pressure versus electrical current curve.

crack closure (phase 2), the borehole pressures for phases 1 and 3 are such that

$$P - P_1 \simeq A\frac{\mathrm{d}t}{\mathrm{d}P} + C \quad \text{for stage I,} \tag{2}$$

$$P - P_2 \simeq B\frac{\mathrm{d}t}{\mathrm{d}P} + D \quad \text{for stage III,} \tag{3}$$

where A, B, C and D are constants which depend on the problem geometry and the material properties. The authors propose to plot $\mathrm{d}t/\mathrm{d}P$ versus P for identifying the pressure P_1 at the end of phase 1, i.e. the pressure reached just before fracture closure starts. However, because of noise associated with the data acquisition system, the computation of the derivative is very noisy and the associated uncertainty is very large. In order to reduce this noise, Eqs. (2) and (3) are integrated:

$$t = \frac{1}{A}\left(\frac{P^2}{2} - P(P_1 + C) + t_1^0\right) \quad \text{for stage I,} \tag{4}$$

$$t = \frac{1}{B}\left(\frac{P^2}{2} - P(P_2 + D) + t_2^0\right) \quad \text{for stage III,} \tag{5}$$

where t_1^0 and t_2^0 are constants.

No derivatives are introduced and the measure is less sensitive to noise. The beginning and the end of the shut-in curve are fitted with quadratic approximations. The departures from the quadratic approximation yield the values P_1 and P_2 reached respectively, at the end of phase 1 (end of fracture propagation) and phase 2 (end of fracture closure). The value of P_1 is supposed to be a good measure of the normal stress acting on the fracture away from the well. Indeed, it corresponds to the pressure when fracture propagation has stopped but before fracture closure has started, i.e. when the fracture is still completely opened and the pressure is uniform up to the fracture tip. It may be outlined that Hayashi and Haimson derivation is only valid for axial hydraulic fractures. However, application to any inclined fracture would only introduce a corrective shape factor without changing the basic trend of pressure decay. Hence, it has been applied to all (HF and HTPF) fractures. Table 2 shows the results obtained with this method.

3.1.2. Determination from electrical signature

Doan and Cornet [22] have proposed to use the electrical signal provided by the HTPF tool as a complementary way to determine the shut-in pressure. Section 2.2 highlighted how the electrical intensity is sensitive to the hydraulic events experienced by the tested fracture.

These data exhibit sharp variations that facilitate the identification of critical pressure values. It is also sensitive to auxiliary effects such as water percolation so that electrical intensity exhibits various surges and drops. In order to discriminate between the various electrical sharp variations, a method coupling hydraulic and electrical data has been proposed.

It is based on the probabilistic representation of experimental results, i.e. the definition of confidence intervals: a given pressure value has only a certain probability to correspond to the real shut-in pressure. This probability is mathematically described by a probability density function (PDF).

The upper right graph of Fig. 9 describes how the PDF of hydraulic shut-in data is built from the simple tangent method. The intersection of the two tangents is often not symmetrically located with respect to the tangential points. The PDF description takes into account this asymmetry: it is approximated by two halves of Gaussian curves. As well pressure versus time varies smoothly with time, the resulting PDF is broad and monomodal.

On the contrary, the electrical PDF signal is characterized by numerous sharp variations. The associated PDF is therefore multimodal but each peak is quite narrow, as shown in Fig. 9. The PDF presented here is the result of the sum of normalized Gaussian function, one for each sharp variation in the electrical curve.

The closure of the fracture is supposed to influence both the electrical and the hydraulic data. This corresponds to a multiplication of their two respective PDFs. The bottom graph of Fig. 9 shows that the process enables a selection of the pertinent electrical event. Here the resulting value P_S^e is both unique and better defined than the hydraulic data alone. This peak can be approximated with a Gaussian bell curve.

Fig. 9 corresponds to the first shut-in of the first test for the Lodève campaign. The method has been applied to all tests of the campaign. While the above algorithm does not guarantee the uniqueness of the data, the computed PDFs are monomodal. Table 2 is then non-equivocally filled. The method gives satisfactory values, compatible with the two other hydraulic tests, with slightly larger error bars.

But, the electrical method does not yield systematically a result, i.e. in some instances, no sharp variation in the electrical current is detected during the shut-in phase. Such a case is illustrated by the third shut-in of Fig. 4. A closer look at the end of the second quasi-static reopening reveals that the intensity decreases twice. A first drop happens before the shut-in. It is as sharp as the variations observed during the first shut-in. At the shut-in stage, the recorded electrical current is then proportional to the declining well pressure. This two-step process might indicate that the propagating fracture has intersected a second fracture and this complicates the fracture closure process. In such an instance, interpretation of hydraulic data is to be conducted with great care. In fact, it might be advisable not to consider the result at all.

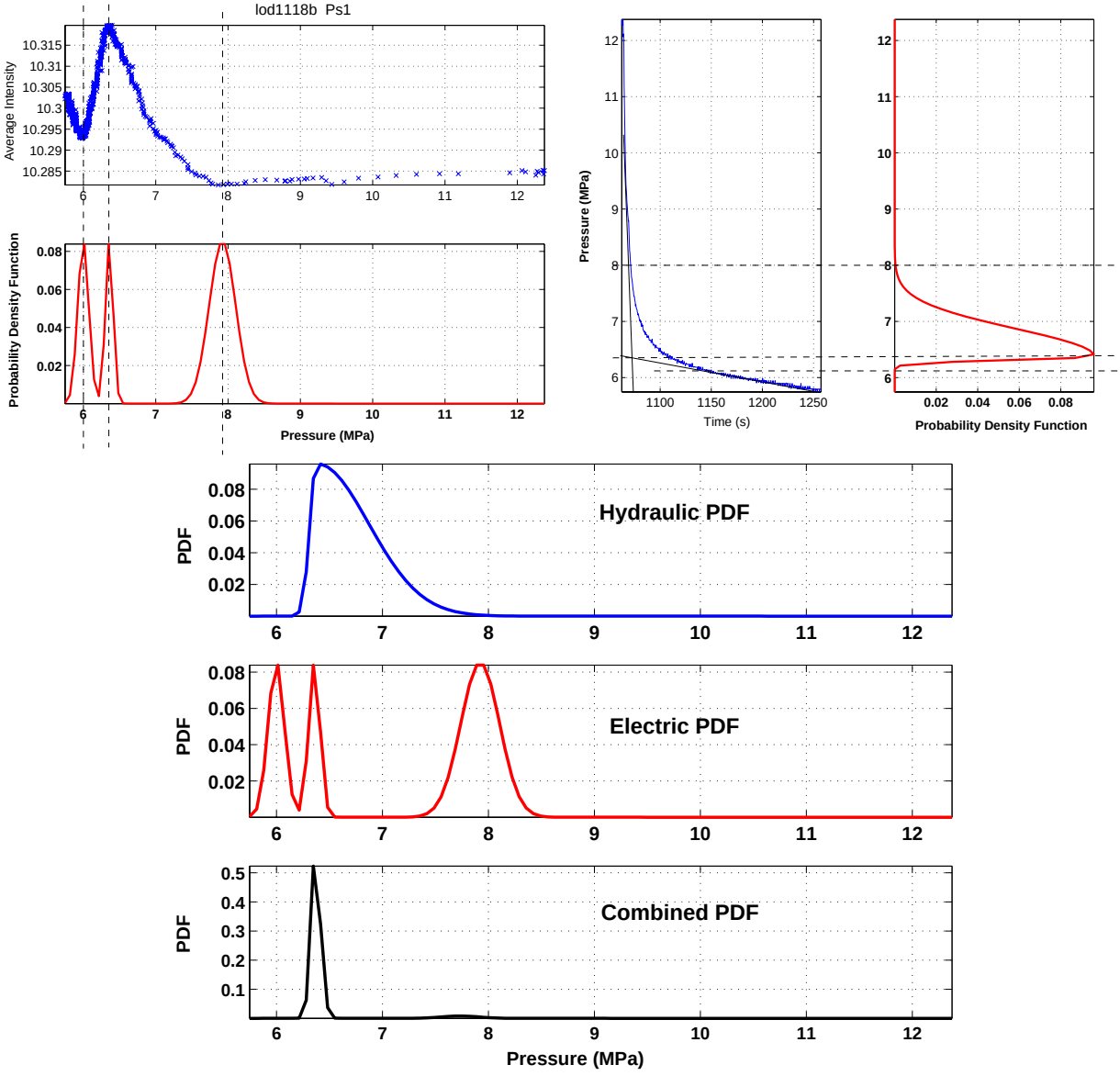

Fig. 9. Principle of determination of PDFs. Upper left: electrical PDF is determined by the summation of normalized Gaussian, centered on the sharp variations of the electrical current. Upper right: the hydraulic PDF is determined through the tangent method. The maximum of PDF corresponds to the intersection of the two tangents. Since it is not equidistant to the departure points of the tangents, the PDF is asymmetric. Bottom: the resulting PDF is the normalized multiplication of the electric and hydraulic PDFs.

3.2. *Determination from quasi-static reopening steps*

Following Cornet and Valette [9], fracture reopening is performed through quasi-static reopening steps. The quasi-static reopening pressure is identified as the transition between two limit hydraulic regimes: flow through a closed fracture governed by the Darcy law, flow through an opened fracture governed by the Poiseuille law.

For each quasi-static step, pressure and flow rate are reported. Results are shown in Fig. 10. The pressure range of the transition zone yields the confidence interval of the reopening pressure.

Observed quasi-static reopening pressures are presented in Table 2. They are affected by high uncertainties given the scarcity of data points for identifying the two flow regimes (generally two or three points for each regime).

It is observed that values of quasi-static reopening pressures, which are supposed to be equal to the normal stress acting on the tested fracture, are systematically higher than the shut-in pressures. Rutqvist and Stephanson [23] and Cornet et al. [24] have also outlined difficulties with quasi-static reopening tests, in particular because of the influence of fracture stiffness. As a consequence of these difficulties, Rutqvist and

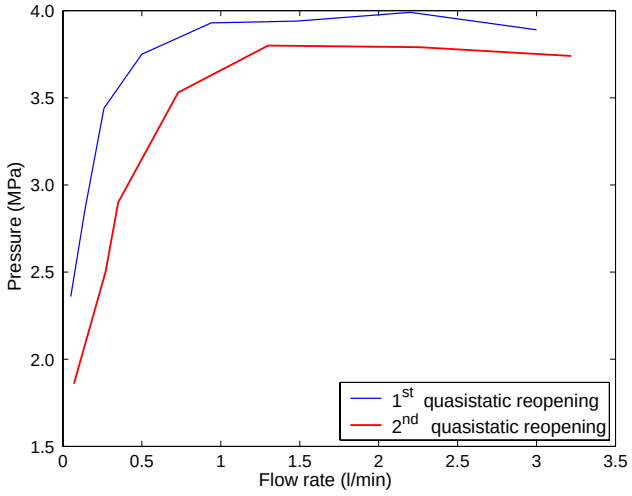

Fig. 10. Pressure versus flow rate for two successive, quasi-static, reopening tests.

Stephanson, propose to measure the normal stress by a quasi-static "closing" process. But Cornet et al. showed that the temporal response of the system, as well as far-field flow conditions, have drastic consequences on the measurement. Hence, it is concluded here that interpretation of these quasi-static reopening tests in terms of normal stress measurements are not accurate and should be discarded.

3.3. Identification of the normal stress supported by the tested fractures

Table 2 presents the results collected with the four methods presented above. As already mentioned, results from quasi-static reopening tests are discarded and only results recorded during the shut-in phase are left to be considered. The first striking feature is that they all are consistent with each other. For any given shut-in phase (for a total of 25 of them), the various values differ by less than one mega Pascal.

Let us recall the basic principles underlying each of the methods. The aim of Aamodt and Kuriyagawa's method is to identify the maximum borehole pressure for which the fracture is completely closed so that flow obeys the Darcy law. This pressure value is an underestimate of the normal stress supported by the fracture. It should be theoretically equivalent to the value defined at the end of Hayashi and Haimson's phase 2 (end of fracture closure). The value P_1 defined at the end of Hayashi and Haimson's phase 1 (end of fracture propagation) is an overestimate of the normal stress supported by the fracture. Finally, the electrical method is supposed to identify the time when the fracture walls just touch each other.

In order to satisfy all these criteria, the following procedure has been followed for identifying the normal stress and the uncertainty associated with the determination. For a given test sequence (three shut-in readings or more), the minimum value obtained with Aamodt and Kuriyagawa's method yields a sure minimum to the normal stress. The maximum value obtained for P_1 with Hayashi and Haimson's method yields a sure maximum to the normal stress. With the electrical method, each shut-in phase yields a confidence interval for the normal stress value. We take the envelope of all these confidence intervals for defining the domain of acceptable solutions for the electrical data. Then we take as final solution the intersection between the hydraulic and the electrical confidence intervals. This is illustrated in Fig. 11. Results (central value and standard deviation) are plotted in the last two columns of Table 2 as well as in Table 3.

4. Complete stress determination

Results that can be used for the stress determination are summarized in Table 3. Clearly, the depth range of measurements (112 m) is too large for neglecting stress gradients. The formation is fairly homogeneous at the scale of tens of meters so that it seems reasonable to postulate a linear variation of stress with depth. Then the stress at depth z is expressed as

$$\underset{\sim}{T}(z) = \underset{\sim}{S} + \underset{\sim}{A}\, z. \tag{6}$$

$\underset{\sim}{S}$ is the stress tensor defined for $z = 0$ and $\underset{\sim}{A}$ is the vertical stress gradient within the depth range of the measurements. They are used to evaluate the complete stress tensor only for depths within the depth range of the tests.

$\underset{\sim}{S}$ and $\underset{\sim}{A}$ are characterized by their three principal values and the orientation of the associated principal directions. Hence, the above parameterization of the stress field implies 12 parameters, but only seven tests have been run: three hydraulic fractures have been developed and four pre-existing fractures have been tested.

The objective is to obtain a complete determination of the stress tensor between 100 and 200 m. The following interpretation procedure has been followed:

(1) The true hydraulic fractures are taken to advantage for determining the principal stress directions and the minimum principal stress magnitude within the corresponding depth range.
(2) Tests on pre-existing fractures are integrated with the results from hydraulic fractures to obtain a complete stress determination at 165 m (six components), independent of any hypothesis on the influence of pore pressure.
(3) An estimate of the vertical gradient of the horizontal maximum principal stress is derived from the

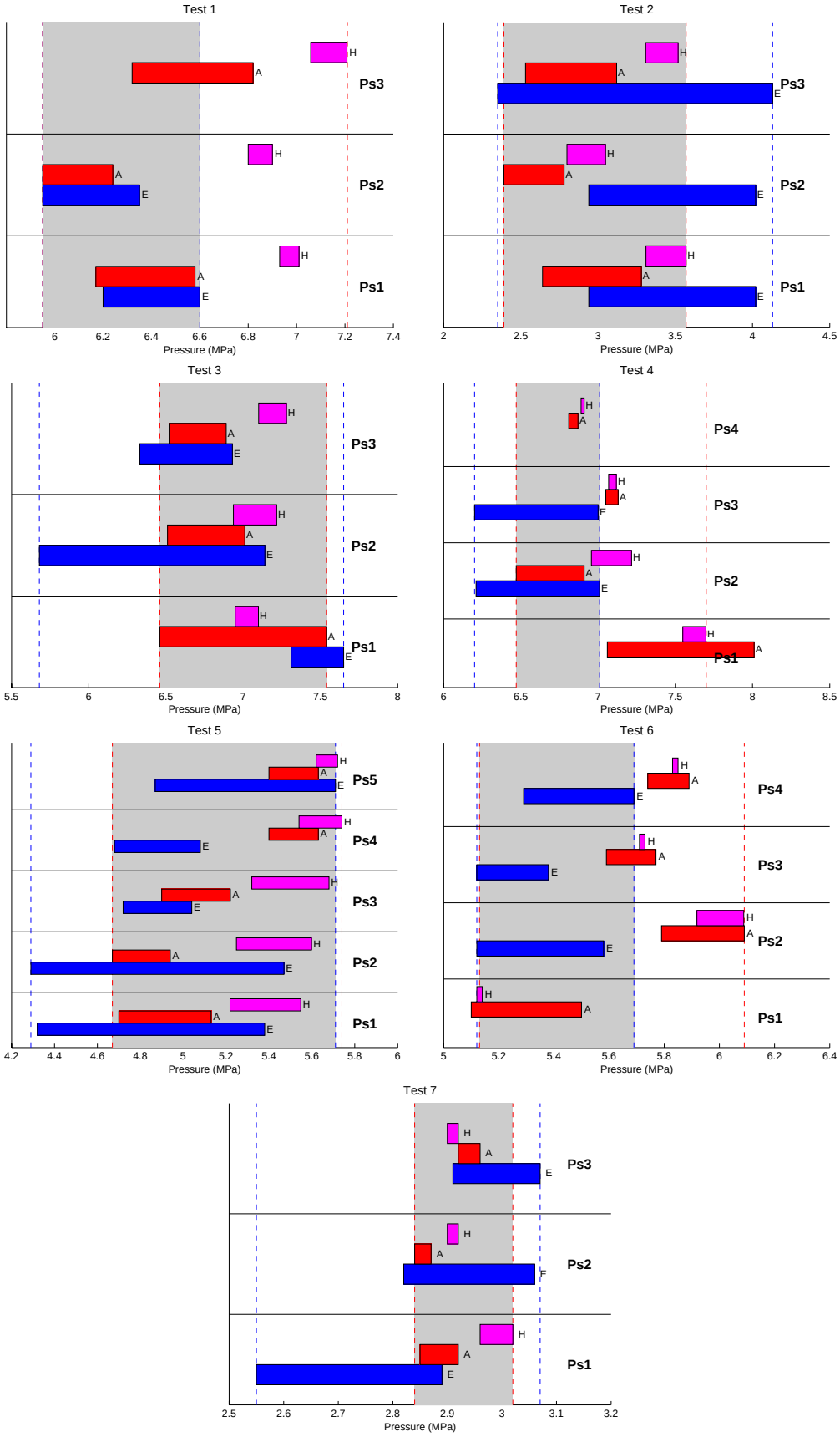

Fig. 11. Determination of normal stress supported by each tested fracture from both electrical (E) and hydraulic data (A: Aamodt and Kuriyagawa; H: Hayashi and Haimson).

Table 3
Synthetic data relative to the hydraulic tests performed during the Lodève campaign

Test	Type	Depth		Azimuth		Dip		Normal Stress		Breakdown
		z (m)	δz (m)	ϕ (°)	$\delta\phi$ (°)	θ (°)	$\delta\theta$ (°)	σ_n (MPa)	$\delta\sigma_n$ (MPa)	P_b (MPa)
1	HF	205	1	230.5	4	90	3	6.3	0.1	12.4
2	HTPF	202	1	183.5	2	33.5	3	3.0	0.2	6.8
3	HTPF	187	1	157	4	42.3	2	7.0	0.2	11.1
4	HTPF	146	1	0.5	2	48	3	6.7	0.2	8.4
5	HF	122	1	242.5	5	90	2	5.2	0.3	10.5
6	HF	106	1	244.5	5	90	3	5.4	0.2	8.8
7	HTPF	93	1	17	2	20	2	2.9	0.1	6.5

Azimuth and dip give the orientation of the normal of the fracture plane.

vertical gradient of breakdown pressures observed during hydraulic fractures. It helps to extrapolate the results obtained at 165 m down to 200 m, and up to 100 m.

The three hydraulic fractures have yielded vertical fractures, which demonstrates that the vertical direction is principal. The mean orientation of the minimum horizontal principal stress is N239$\pm$11°E (99% confidence level). The value of the minimum principal stress at 110 m is taken equal to the mean value between the two tests at 106 and 122 m; i.e. 5.3$\pm$0.3 MPa. This yields a vertical gradient for the minimum horizontal principal stress equal to 0.011 MPa/m, with a negligible effect of the uncertainty on the gradient, given the depth range of the measurements and the uncertainty on the magnitude of the minimum horizontal principal stress. Hence, the HF tests provide four of the stress components at any depth between 100 and 200 m, or eight out of the 12 parameters required for describing the stress field and its variations with depth. Indeed, we have assumed that there is no significant rotation of principal directions within the depth range of interest, i.e. the 14° difference between the bottom HF and the most superficial one is considered to be caused by local heterogeneity. This leaves four parameters to be determined from the four tests on pre-existing fractures and this is still not acceptable, given the uncertainties on the measurements.

Further, examination of results obtained at 202 m shows that this test has not been successful. Indeed, from the electrical image it is clear that the straddled interval was set on a pre-existing fracture (see Fig. 5). Variations in electrical resistivity during the test do not show the opening of the observed fracture, but rather that of a localized channel. The final electrical image of the fracture shows a contrasted change in electrical resistivity, with an increase in its upper part and a decrease in its lower part, suggesting some shear motion. Finally, the value obtained for the normal stress (3.0 MPa) is much smaller than that anticipated for the vertical component, which is the minimum principal stress component at this depth. Indeed, with a mean rock density of 2.4 for these sedimentary rocks (a value of 2.9 has, in fact, been measured for some of the pellites) would yield a vertical component equal to 4.8 MPa, i.e. a value much larger than that which has been measured. Given the initial strong hydraulic conductivity and the fact that the test interval pressure reaches back the hydrostatic borehole pressure during the shut-in tests, it is concluded that results from this test are to be discarded.

This leaves three HTPF tests for the determination of the four remaining parameters. The problem is to determine these parameters from normal stress magnitudes measured on three fractures with known orientation $\vec{n}$, described by its azimuth ϕ and dip θ:

$$\sigma_n = \vec{n} \cdot \underset{\sim}{T} \cdot \vec{n}. \tag{7}$$

Inserting Eq. (6) into Eq. (7) yields

$$\sigma_n^m - A_3 x_3^m \cos\theta_m - \frac{\sin^2\theta_m}{2}(S_1 + S_2 + (A_1 + A_2)x_3^m + (S_1 - S_2)\cos 2(\phi_m - \lambda) + (A_1 - A_2)\, x_3^m \times \cos 2[\phi_m - (\lambda + \eta)]) = 0, \tag{8}$$

where S_i (resp. A_i) are the principal values of tensor $S_\sim$ (resp. $A_\sim$). λ is the orientation of S_1, while η is the orientation of A_1 with respect to that of S_1.

Given the absence of strong topography, the subhorizontality of sedimentary layers, and the fact that the vertical direction has been shown to be principal, it has been assumed that the vertical component is equal to the weight of overburden. In Eq. (6), the vertical principal component of $S_\sim$ is null and this leaves only three unknowns to be determined. From the dip of the pre-existing fractures, it is clear that only the tests at 187 and 146 m are amenable to constraining the maximum horizontal principal stress. Given their small depth difference, we neglect local vertical variations of the maximum horizontal stress.

This leaves only two unknowns, i.e. the mean rock mass density and the maximum horizontal principal stress at 165 m. Possible solutions have been identified

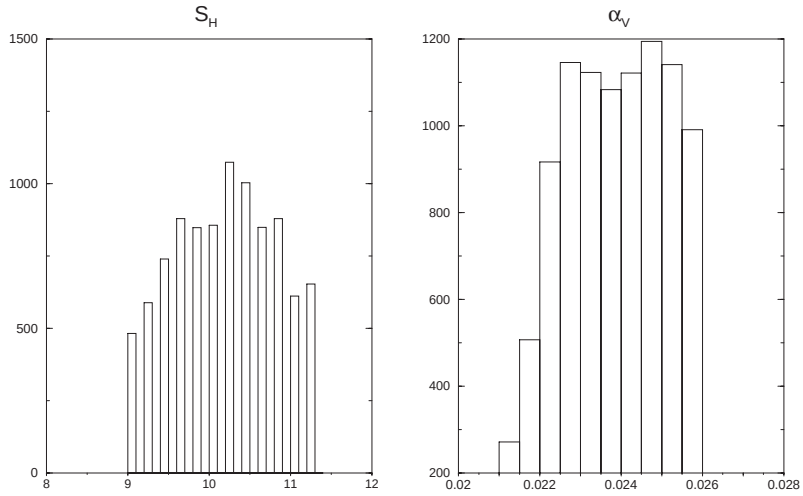

Fig. 12. Results for the horizontal maximum principal stress and the mean vertical stress gradient from a Monte-Carlo exploration of the solution space. The azimuth of S_1 has been set equal to 155°.

with a Monte-Carlo method for exploring the complete set of possible solutions. The discrepancy between the computed normal stress

$$\sigma_{\mathrm{n}}^{c}(\sigma_{\mathrm{H}}, \alpha_V, \vec{n}^m) = \vec{n}^m \cdot \underset{\sim}{T}(\sigma_{\mathrm{H}}, \alpha_V) \cdot \vec{n}^m \tag{9}$$

and the errors on measured value σ_{n}^{m} are summed on all tests to obtain the following misfit function:

$$\sum(\sigma_{\mathrm{H}}, \alpha_V) = \sum_{m=1}^{N} \left| \frac{\sigma_{\mathrm{n}}^{c}(\sigma_{\mathrm{H}}, \alpha_V, \vec{n}^m) - \sigma_{\mathrm{n}}^{m}}{\delta\sigma_{\mathrm{n}}^{c} + \delta\sigma_{\mathrm{n}}^{m}} \right|. \tag{10}$$

$\delta\sigma_{\mathrm{n}}^{c}$ reflects the uncertainty on σ_{n}^{c} because of uncertainties on fracture orientation $\vec{n}^m$. A first exploration of the parameters space is performed to get an estimate of the minimum of the misfit function, here $\sum_{\min} = 2.34$. The parameters consistent with the 50% confidence level exhibit a misfit value lesser than $\sum_{50} = (0.676(\pi/2 - 1)^{1/2} N^{1/2} + N/(N-K))\sum_{\min} \sim 4.35$ where K is the number of degrees of freedom [25]. Fig. 12 presents a statistics of such values provided by a second Monte-Carlo exploration on 10 000 random samples. The average value of each histogram gives the expected value of the corresponding parameter. The standard deviation of the distribution gives an estimate of the uncertainty of the results.

The values pointed out by Monte-Carlo method may then be chosen as a priori values for identifying the best solution with the Tarantola–Valette least-squares algorithm [26,9]. It provides a rigorous estimate of the confidence interval of the final results. The full stress tensor is obtained at $z = 165$ m. The vertical direction is a principal stress direction and $S_{\mathrm{v}} = 4.0 \pm 0.5$ MPa. The maximum horizontal principal stress component is oriented to $\mathrm{N} - 25° \pm 1°\mathrm{E}$ and equals $S_{\mathrm{H}} = 10.0 \pm 0.2$ MPa. It is almost twice the value found for S_{h}, $S_{\mathrm{h}} = 5.8 \pm 0.1$ MPa. The mean rock density is measured to be 0.025 MPa/m.

In order to obtain the stress components at 200 m, the mean vertical gradient of the maximum horizontal principal stress is evaluated from the breakdown pressure. Indeed, at depth z, the breakdown pressure is given by [6]

$$KP_{\mathrm{b}} = 3\sigma_{\mathrm{h}}(z) - \sigma_{\mathrm{H}}(z) + \sigma^{\mathrm{T}} - K'\rho_w g z, \tag{11}$$

where

- $$K = \begin{cases} 1 & \text{for impervious formation (no fluid percolation),} \\ 2 - \alpha\frac{1-2v}{1-v} & \text{for permeable rocks,} \end{cases}$$

  where v is the bulk material Poisson's ratio and α is Biot's coefficient $(1 - K_{\mathrm{b}}/K_{\mathrm{M}})$ in which K_{b} and K_{M} are, respectively, the compressibility of the bulk material and that of the rock matrix.
- $$K' = \begin{cases} O & \text{when the pore pressure is ignored,} \\ 1 & \text{when the rock mass has some porosity but the borehole fluid percolation is ignored,} \\ \alpha\frac{1-2v}{1-v} & \text{when fluid percolation is taken into consideration.} \end{cases}$$

Eq. (11) outlines the difficulty in properly taking into account effects of pore pressure and its variation induced by the injection tests. Many hypotheses must be formulated (penetration or no penetration of pore fluid, influence or no influence of pore pressure on

tensile strength). Additional measurements must be conducted (Poisson's ratio and compressibility modulus for the bulk material and compressibility for the rock matrix). Further, permeability is assumed to be independent of stress. Clearly, when Eq. (11) is used for the determination of the magnitude of $\sigma_H(z)$, the precision of the determination is not as good as that of the minimum principal stress component.

Interestingly, when Eq. (11) is applied to the three hydraulic fracturing tests, it is found that the correction for pore pressure must be neglected if the gradient of the maximum horizontal principal stress is to be positive. Then, its mean value is equal to 0.002 MPa/m. This small value shows that, in fact, the effect of the stress gradient between 165 and 200 m remains negligible, given the uncertainty on the stress determination. It implies a value of $S_H = 8.8$ MPa around 100 m.

5. Discussion

Electrical measurements run during the various hydraulic tests have all shown an increase in electrical intensity, outlining a decrease in electrical resistivity of the system. This suggests that some percolation process that induced some changes in pore pressure around the well bore has occurred. Yet, considerations on the gradient of breakdown pressure suggests that pore pressure effects should remain negligible. In the absence of data on the various physical quantities involved (electrical resistivity of formation fluid and injected water, permeability of the rock, compressibility of the rock matrix and of the bulk material), the analysis of the exact role of variations in pore pressure cannot proceed further. But an important observation is that images of variations of the borehole wall electrical resistivity show that these are not evenly distributed. This raises the question of properly taking into account the influence of local heterogeneity on pore pressure perturbation near the well. Clearly, the advantage of combining HF and HTPF for our stress determination has suppressed limitations caused by the poor understanding of pore pressure effects. Further, it has provided a determination of all components, including the vertical component.

The amount of tests run on this site is fairly representative of most field measurements by hydraulic testing. Yet this amount remains too small for appraising efficiently the stress variability within the tested volume. Although the mathematical evaluation of uncertainty indicates a satisfactory resolution, the influence of the implicit assumption of stress continuity is not evaluated. This evaluation would have implied a much larger number of tests. However, some evaluation of the significance of the results may be obtained by comparing results to other stress measurements conducted nearby, as well as to regional geological indicators of principal stress.

Stress measurements have been conducted by hydraulic testing at Tournemire, some 40 km to the north-west of the site [27]. A N162 $\pm$ 15°E orientation has been determined for this site. Also, as can be seen in Fig. 1, an alignment of volcanoes (dated early quaternary) extends in the north–south direction, some 20 km to the west of the site. This is often interpreted as the surface expression of a deep elongated magma chamber, the orientation of which is similar to that of a long hydraulic fracture. So, it is concluded that the regional stress field in this area is oriented somewhere between N–S and NNW–SSE.

Interestingly, Burlet [28] has reported results obtained at Merifons some 21 km to the south-west of the site. He conducted 15 hydraulic tests at depth ranging from 257 down to 840 m. The magnitude of the minimum horizontal principal stress and its vertical gradient (5.3 MPa at a depth of 160 m, with a vertical gradient equal to 0.014 MPa/m) are found to be very similar to the values reported in this paper. But the orientation of the minimum horizontal principal stress is found to be exactly orthogonal (N254°E). One may question whether this difference in stress orientation is real or whether some error has been made in the data reporting (like inverting the orientation of the planes with that of their normal).

From the hydrogeological perspective, four main fracture and fault directions are identified on site [8]: two directions (N–S and N30°E) are producing water, while two directions (N100°E and N130°E) are acting as barriers. Faults are differentiated from fractures by their size normally longer than 1 km and by the relative displacement usually larger than 100 m. It has sometimes been reported that, in tectonically active domains, the main flowing fractures exhibit orientation consistent with the largest Coulomb stress [29,30]. If these concepts are to be applied to the present site with the stress field reported in this paper, the two directions N30°E and N130°E should be producing water, when in fact the N130°E direction is identified as a strong barrier. However, recent results obtained in the Corinth Rift, in Greece, have shown that the main normal faults of this rift are acting as strong hydraulic barriers, because of clay smearing effects [31]. A similar conclusion had been reached for the permeability of the 1200 km long Philippine fault [32], which is a transform fault. Clearly, the hydraulic behavior of fractures (arbitrarily defined as discontinuities with length shorter than 100 m) is different from that of faults. For the latter, the filling (or gouge) material depends strongly on their past history as well as on the geochemistry of fluids which have percolated through them, so that their hydraulic conductivity do not depend solely on their relative orientation with respect to the stress field.

6. Conclusion

The stress determination campaign which has been conducted in the sedimentary pellitic formation of Lodève, has been successfully completed by integrating results from hydraulic fracturing and from hydraulic tests on pre-existing fractures. It has provided all the necessary information for a complete stress tensor determination at the depth of 165 m. This determination concerns the total stress and does not require any understanding of pore pressure effects. The determination of the principal stress magnitudes rests on an accurate measurement of the normal stress of either true hydraulic fractures or pre-existing fractures.

This normal stress measurement has greatly benefited from the real-time electrical well bore imaging achieved during hydraulic testing. Electrical imaging provides both, an understanding of the geometry of zones where flow occurs and means to identify the time when a hydraulically opened fracture closes back during shut-in. It also provides the necessary preliminary log for selecting location of the tests. It ensures that hydraulic tests are conducted precisely on the selected intervals. Finally, comparison between results obtained during shut-in periods and quasi-static reopening test shows that the latter yields systematically values larger than that of the shut-in tests. They have been discarded for this stress determination.

Principal stress directions identified on this site are consistent with the results obtained on a site located, respectively, about 40 km from the present site, as well as with the geological markers (volcanoes alignment). These results suggest that flow through the natural fault and fracture system, as observed at ground surface and down to 300 m does not depend strongly on this regional stress field. The morphology of the fault system together with the nature of the material filling the faults appears to be of stronger influence.

Acknowledgements

We wish to acknowledge J.P. Petit, Department of Geology, University of Montpellier II, who provided the support for this investigation. Our thanks to Y. Wileveau, B. Bert and G. Rozières who conducted the hydraulic tests on site.

References

[1] Haimson BC, Fairhurst C. Initiation and extension of hydraulic fractures in rock. Soc Petr Eng J 1967;7:310–8.

[2] Haimson BC. The hydraulic fracturing method of stress measurement—theory and practice. In: Hudson JA. editor. Rock testing and site characterization. Comprehensive Rock Engineering, vol. 3, Oxford: Pergamon Press, 1993. 395–412 [Chapter 14].

[3] Daneshy AA. A study of inclined hydraulic fractures. Soc Petr Eng J 1973;13:61–8.

[4] Richardson RM. Hydraulic fracture in arbitrarily oriented boreholes: an analytic approach. In: Zoback MD, Haimson B, editors. Hydraulic fracturing stress measurements. Washington DC: National Academy Press; 1983. p. 167–75.

[5] Bredehoeft J, Wolff R, Keys W, Shuter E. Hydraulic fracturing to determine the regional in-situ stress field, Piceance basin, Colorado. Geol Soc Am Bull 1976;87:250–8.

[6] Schmitt DR, Zoback MD. Poroelastic effects in the determination of the maximum horizontal principal stress in hydraulic fracturing test—a proposed breakdown equation employing a modified effective stress relation for tensile fracture. Int J Rock Mech Min Sci Geomech Abstr 1989;26(6):499–506.

[7] Evans KF, Cornet FH, Hashida T, Hayashi K, Ito T, Matsuki K, Wallroth T. Stress and rock mechanics issues of relevance to HDR/HWR engineered geothermal systems: review of developments during the past 15 years. Geothermics 1998;28: 455–74.

[8] Bruel T. Caractérisation des circulations de fluides dans un réseau fracturé et rôle des contraintes in situ. Une étude de cas dans le bassin permien de Lodève. Ph D thesis, Université de Montpellier II, 1997.

[9] Cornet FH, Valette B. In situ stress determination from hydraulic injection test data. J Geophys Res 1984;89(B13):11527–37.

[10] Cornet FH. Stress determination from hydraulic tests on preexisting fractures—the H.T.P.F. method. In: Stephansson O, editor. Proceedings of the International Symposium on Rock Stress and Rock Stress Measurements, Lulea, 1986. CENTEK Publ. p. 301–11.

[11] Doe TW, Korbin GE. A comparison of hydraulic fracturing and hydraulic jacking test measurements. In: 28th US Symposium on Rock Mechanics, Tucson, AZ. 29th June–1st July,1987, Boston, MA, Rotterdam: A.A. Balkema, 1987. p. 283–90.

[12] Baumgartner J, Rummel F. Experience with "fracture pressurization tests" as a stress measuring technique in a jointed rock mass. Int J Rock Mech Min Sci Geomech Abstr 1989;26(6):661–71.

[13] Turnbridge LW. Interpretation of the shut-in pressure from the rate of pressure decay. Int J Rock Mech Min Sci Geomech Abstr 1989;26(6):457–9.

[14] Cornet FH, Wileveau Y, Bert B, Darcy J. Complete stress determination with the HTPF tool in mountainous region. Int J Rock Mech Min Sci 1997;34(3–4).

[15] Mosnier J. Détection électrique des fractures naturelles ou artificielles dans un forage. Ann Géophys 1982;38:537–40.

[16] Mosnier J, Cornet F. Apparatus to provide an image of the wall of a borehole during a hydraulic fracturing experiment. In: Louwrier K, Staroste E, Garnish JD, Karkoulias V, editors. Fourth International Seminar on the Results of EC Geothermal Energy Research and Demonstration, Proceedings, Dordrecht: Commission of the European Communities, Kluwer Academic Publishers; 1989. p. 205–12.

[17] Cornet FH. The HTPF and the integrated stress determination methods. In: Hudson JA, editor. Rock testing and site characterization. Comprehensive rock engineering, vol. 3 Oxford: Pergamon Press, 1993; p. 413–32 [chapter 15].

[18] Wileveau Y. Mesures du champ de contrainte dans les milieux complexes par la méhode HTPF. Naissance d'une sonde. PhD thesis, Univ D Diderot Paris VII, 1997.

[19] Hayashi K, Haimson BC. Characteristics of shut-in curves in hydraulic fracturing stress measurements and the determination of the in situ minimum compressive stress. J Geophys Res 1991;96(B11):18311–21.

[20] Guo F, Morgernstern NR, Scott JD. Hydraulic fracturing pressure: a comparison of eight methods used to identify shut-in pressure. Int J Rock Mech Min Sci Geomech Abstr 1993;30:627–31.

[21] Aamodt RL, Kuriyagawa M. Measurement of instantaneous shut-in pressure in crystalline rock. In: Zoback MD, Haimson B, editors. Hydraulic fracturing stress measurements. Washington, DC: National Academy Press; 1983. p. 139–42.
[22] Doan ML, Cornet FH. A coupled hydraulic and electrical stress determination technique. In: Hammah R et al. editor. Mining and tunneling innovation and opportunity, vol. 2, NARMS-TAC, University of Toronto Press; Toronto, 2002. p. 1413.
[23] Rutqvist J, Stephansson O. A cyclic hydraulic test to determine the in-situ stress normal to a fracture. Int J Rock Mech Min Sci Geomech Abstr 1996;33(7):695–711.
[24] Cornet L, Li FH, Hulin JP, Ippolito I, Kurowski P. The hydromechanical behaviour of a fracture: an in situ experimental case study. Int J Rock Mech Min Sci 2003; this volume.
[25] Parker RL, McNutt MK. Statistics for the one-norm misfit measure. J Geophys Res 1980;85(B8):4229–430.
[26] Tarantola A, Valette B. Generalized nonlinear inverse problems solved using the least squares criterion. Rev Geophys 1982; 20(2):219–32.
[27] Cornet FH. Détermination du champ de contrainte au voisinage du laboratoire souterrain de Tournemire. Technical report, IPSN Contract no: 4060 9B038960/SH, April 2000.
[28] Burlet D. Détermination du champ de contrainte régional à partir de tests hydrauliques en forage. PhD thesis, Univ Paris VII, 1991.
[29] Barton CA, Zoback MD, Moos D. Fluid flow along potentially active faults in crystalline rock. Geology 1995;23(8):683–6.
[30] Ito T, Zoback MD. Fracture permeability and in situ stress to 7 km depth in the KTB scientific hole. Geophys Res Lett 2000;27(7):1045–8.
[31] Cornet FH and the Corinth-Rift-Lab team. Drilling the Aegion fault of Corinth Rift Laboratory. In: EGS-AGU-EUG Joint Assembly, Nice France, 06–12 April 2003, 2003.
[32] Prioul R, Cornet FH, Dorbath C, Dorbath L, Ogena M, Ramos E. An induced seismicity experiment across a creeping segment of the Philippine fault. J Geophys Res 2000;105(B6): 13595–612.